Analysis of throat heat transfer in GOX/GCH_4 liquid rocket engines

Pierluigi Concio*
Sapienza University of Rome, 00184 Rome, Italy

This work aims mainly to investigate the steady-state flow field and heat flux profile along the thrust chamber by means of RANS based CFD numerical simulations. Attention is paid on the throat and on how, for the sake of simplicity, a non detailed injection of propellants at chemical equilibrium can be a reasonable simplification within CFD predictions. In order to perform comparisons, full modeled calculations are taken from literature as well as from Technische Universität München (TUM) experimental tests on a capacitively cooled square-rectangular shape single element and, with more interest, an axisymmetric 7 element film cooled rocket combustors. The contribution of near-wall chemical recombinations to heat flux is investigated according to a frozen kinetics and species mass fraction profiles are considered in order to observe deviations from chemical equilibrium. The numerical convective heat flux is further employed to verifying the reliability of isothermal boundary conditions on the nozzle walls and to have a comparison with the radiative contribution. Having the experimental averaged heat flux at the throat as a reference, the numerical solution returns an error of 12%**, fully comparable with the order of magnitude typical of more expensive and sophisticated methods. Nevertheless, combustion efficiency turned out to be responsible of a significative lack of modeling as mainly stated by a parametric analysis with varying chamber length.**

I. Nomenclature

x	=	abscissa	h_g	=	hot gas side convective heat transfer coefficient
k	=	thermal conductivity	$\nabla(\cdot)_n$	=	gradient in the normal direction
δ	=	thickness	r	=	solver spacial order of accuracy
L_{cc}	=	combustion chamber length	f_{rex}	=	Richardson extrapolated solution
T	=	temperature	f_{fine}	=	fine grid solution
T_w	=	wall temperature	f_{medium}	=	medium grid solution
T_{aw}	=	adiabatic wall temperature	RTE	=	Radiative Transfer Equation
T_{wr}	=	wall temperature thermocouple reading	TCI	=	Turbulence-Chemistry Interaction

II. Introduction

In liquid rocket engines the quantification of the throat heat load is essential for sizing purposes, as it represent the maximum amount of heat flux exchanged in the entire engine. The high adiabatic wall temperatures (even 3500 K) let thermal power release be a significant concern in keeping the walls within their temperature admissible range in such applications, evaluable around 800 - 900 K for copper-based alloys. As a consequence, an intense chamber cooling capable to extract high heat fluxes is required. Thanks to the capability to withstand higher heat fluxes and provide adequate cooling through high thermal conductivities, the aforementioned copper-based alloys are considered since the last decades of the last century a good choice for the chamber walls material with respect to stainless steel for example [1]. The cooling system plays a fundamental role in deciding how much an investigation on heat loads can be challenging. Capacitively cooled thrust chambers turned out to be the most challenging ones due to the limited amount of measurements allowed by the melting temperature of thermocouple materials. Among the studies conducted on such thrust chambers[2–4], a subscale version was employed Haidn et al. in order to experimentally document the detailed wall heat flux characteristic of a gaseous oxygen/gaseous methane shear coaxial single element injector over a range of pressures and mixture ratios [4]. As said before, technological limits prevented measurements within the nozzle,

*MSc student, Department of Mechanical and Aerospace Engineering, Via Eudossiana 18.

whereas results on the cylindrical part were carried out lengthwise in terms of heat flux and static pressure profiles. In order to overcome this limitation, an active cooling system turned out to be a solution since no termocouples are needed anymore in the nozzle. In this regard the total enthalpy difference between the outgoing and incoming coolant flow can provide an indirect measurement of the heat flux at throat, as done by Haidn et al. on a 7 element methane fueled combustor [5]. With regard to propellants, methane has been recently considered as a valid low cost replacement to other hydrocarbons, thanks to its higher specific impulse and cooling efficiency, cleaner and non toxic exhaust products and better combustion properties through lower viscosity and higher specific heat capacity [6, 7]. Higher coking and sooting limits make oxygen/methane propellant combination a good solution for reusability issues for fly back boosters within the area of RLV [6]. In comparison with hydrogen, methane can also rely on more affordable costs, a more permissive boiling point for a longer storage and a well comparable bulk density impulse [8].
Many studies have been published in literature in order to provide numerical results relying on a detailed injection process and experimental data as a reference [9–12]. High computational costs were involved, of the order of millions of cells. Both in-house and commercial CFD solvers were employed according to different turbulence closure and TCI modeling. ε and ω-based models have been a common choice for turbulence, whereas TCI have been mainly modeled according to a laminar flame model or a β-shaped pdf. It has been observed how the β-shaped pdf approach tends to "smoothen" the temperature field and the ε-based models predict a stronger mixing and hence a thicker flame with a previous impingement point at the wall, resulting in flat-looking trends upstream to the nozzle [10, 11]. Since neglecting injection and combustion details is a reasonable simplification sufficiently downstream of the injector plate, this work focuses its attention on the effect of non detailed propellant injection in order to make a compromise between computational cost and a detailed resolution. In particular, a full flow inlet lets gaseous propellants enter in the combustion chamber. This kind of injection allows to understand the effect of combustion and injection itself on the heat flux, in particular by how much the more expensive usual result differs from the full flow one and quantify if these processes can be reasonably neglected only for the analysis at the throat. A similar thing is intented to be done also with chemical recombinations in order to visualize their contribution to heat flux besides combustion.

III. Test specimens description

A. Single element combustor

This experimental test [4] employs a 3 segments square shape thrust chamber. Two segments, respectively 174 *mm* and 145 *mm* long, made up the 12 *mm* x 12 *mm* inner cross section combustion chamber. The nozzle, represented by the 20 *mm* long last segment, differs from a usual configuration due to its throat with a rectangular cross section of 4.8 *mm* x 12 *mm*, which results in a contraction ratio of 2.5 and Mach number in the chamber of 0.24. The throat is flat and of 1 *mm* length. In order to keep the design more accessible for temperature measurements, the oxygen-free copper (Cu-HCP) thrust chamber is capacitively cooled [4]. The operating point chosen for this test is identified by a chamber pressure of 20 *bar* and a mixture ratio of 2.6, resulting in a total mass flow rate of 0.062 kg/s.

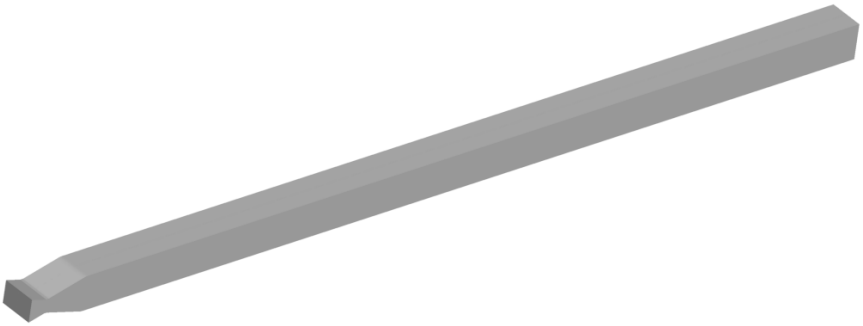

Fig. 1 Single element combustor geometry.

A suitable sensoring enriches the assembly, in particular several pressure transducers and thermocouples are used. Aside from pressure sensors, employed especially for a better understanding of the complex heat release and combustion processes, the temperature field is determined by means of 34 thermocuples, mounted according to specific patterns in the chamber walls. In order to characterize the heat flux within the chamber wall, some thermocouples are clustered in

triplets with different distance from the first segment upper side hot wall. On both the side and the top wall is imposed a specific wall temperature distribution. A combustion efficiency of 98.4% has been evaluated by taken as a reference the faceplate to throat chemical equilibrium characteristic velocity.

B. 7 element combustor

The axisymmetric seven-element rocket combustion chamber is comprised of four cylindrical water cooled chamber segments, one long and three short segments, and a nozzle segment for a total length of $341 + 42$ *mm*. The latter features also an inner diameter of 30 mm and a throat diameter of 19 *mm*, reulting in a contraction ratio of 2.5. In order to easily scale the chamber with the injector dimensions, the distance between the injectors as well as the injector-wall-distance are kept constant and equal to half of the injector diameter, which leads to a pattern of seven injector elements [5]. Since this work is not interested in, further injector's features are left to the reader ([5]). The operating point chosen for this test case employs a mean combustion chamber pressure of 18.3 *bar* and a mixture ratio of 2.65. With a total mass flow rate of 0.291 kg/s, this chamber features a combustion efficiency of 94.5 %, calculated according to the same procedure used for the previous case.

Fig. 2 7 element combustor geometry.

One of the key aspects of the project is to improve the knowledge on heat transfer processes and cooling methods in the combustion chamber, which is mandatory for the engine design. In order to accomplish that, the entire assembly is film cooled by means of the aforementioned two water channels. A single water channel would not have been appropriate due to the too much high temperature at the outlet of the fourth segment. For the determination of the thermal loads a calorimetric method is applied. The heat rate to each chamber segment is determined by the difference of the coolant total enthalpy between inlet and outlet [5].

IV. Numerical method and computational setup

A. Numerical approach

Steady-state numerical simulations have been conducted on the hot gas sides by means of the AFFS in-house three dimensional finite volume Reynolds Averaged Navier-Stokes (*RANS*) equation solver. The latter is second-order accurate in space and able to treat multicomponent mixtures of thermally perfect gases, which can evolve in the flowfield according to the JL-R finite rate chemical reaction mechanism [13], shown in the following table.

Table 1 JL-R model reactions (units in calories, moles,centimeters and seconds) [14].

Number	Reactions	Rates
1	$CO + H_2O \rightleftharpoons CO_2 + H_2$	$r_1 = 2.75 \cdot 10^{12} e^{-20000/RT}[CO][H_2O]$
2	$H_2 + \frac{1}{2}O_2 \rightleftharpoons H_2O$	$r_2 = 1.21 \cdot 10^{18} T^{-1} e^{-40000/RT}[H_2]^{0.25}[O_2]^{1.50}$
3	$O_2 \rightleftharpoons 2O$	$r_3 = 1.5 \cdot 10^{9} e^{-113000/RT}[O_2]$
4	$H_2O \rightleftharpoons H + OH$	$r_4 = 2.3 \cdot 10^{22} T^{-3} e^{-120000/RT}[H_2O]$
5	$OH + H_2 \rightleftharpoons H + H_2O$	$r_5 = 2.10 \cdot 10^{8} T^{1.51} e^{-3430/RT}[OH][H_2]$

Since a 8 species chemistry has been used in this contest, the two irreversible reactions which take into account for methane have been removed. Time integration is done using the Strang operator splitting technique. The convective and diffusive terms are integrated using a second order accurate Runge-Kutta scheme, whereas the chemical source term is integrated using a stiff ordinary differential equation implicit integrator [13]. Turbulence is described by means of the Spalart-Allmaras one quation model, where constant turbulent Schmidt and Prandtl numbers ($Sc_t = 0.7$ & $Pr_t = 0.9$) model respectively turbulent diffusivity and conductivity. Mixture thermodynamic and transport properties as well as

chemical kinetic rates are evaluated as a function of the local temperature and composition. The values are evaluated for each species at different temperatures and stored in lookup tables to reduce the computational cost of each time step. The mixture value of each thermodynamic property is evaluated as the weighted sum of the value of each species by means of the species mass fraction. The mixture value of the transport properties is evaluated by means of Wilke's mixing rule [13]. Wall heat flux is evaluated as the conductive heat transfer between the fluid volume near the wall and the wall itself, because the fluid at the wall is characterized by zero velocity. Wall heat flux can be expressed by Fourier's law as the prodict of the thermal conductivity and the temperature gradient normal to the wall: $q_w = k(\nabla T)_n$. The radiative heat flux is evaluated by integrating the RTE [15] and therefore the radiative intensity at the wall over all the thrust chamber.

B. Computational grids and boundary conditions

CFD simulations have been carried out respectively by means of a three dimensional and a two dimensional axysimmetric grid as shown in fig.3. In both cases, cells are clustered toward the wall in the radial direction in order to solve properly the viscous sublayer of the boundary layer [13]. Moreover, cells are suitably clustered also toward the throat abscissa from both left and right directions in order to have locally the smoothest heat flux profile as possible. Grids have been designed in order to have a nondimensional wall distance of about 1 along the entire chamber for the employed grid level. The latter is made up by $160 \times 60 = 9600$ cells for the 7 element combustor and $200 \times 30 \times 30 = 1.8 \cdot 10^5$ cells for the other one. For the 7 element combustor fine and coarse levels for grid convergence are inferred simply by doubling and halving the grid cells in all directions. In the other case, for the sake of computational cost, medium and coarse levels are obtained by halving once and twice.

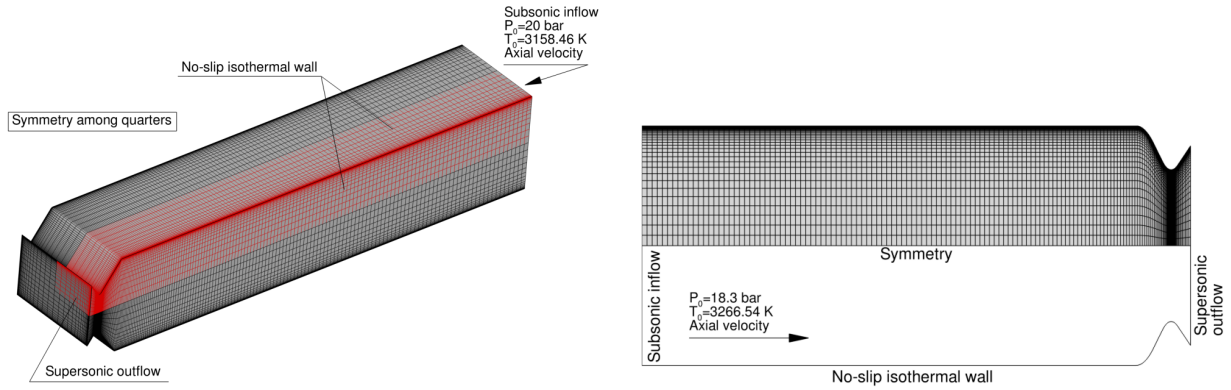

(a) **(b)**

Fig. 3 Computational grids (not to scale) with boundary conditions. (a) Single element combustor; (b) 7 element combustor.

Stagnation pressure, stagnation temperature, mixture composition and velocity direction are enforced at the inlet boundary, in particular propellants are injected along the axial direction according to their chemical equilibrium composition. The outflow is supersonic, therefore no conditions have to be enforced. Internal connections, i.e. planes of symmetry, are modeled using the symmetry boundary condition. The upper wall is set as a no-slip one, as well as isothermal and non catalytic, hence no species gradient contribution has to be added to the wall heat flux evaluation [13]. A wall temperature of 412 K has been enforced on the 7 element combustor grid, whereas an average of the experimental measurements has been employed on the single element one. Being three dimensional, the latter features a top and a side wall, whose boundary condition are slightly different. An average wall temperature of 417.37 K and 415.87 K has been enforced respectively on the top wall and on the side wall. After the simulation, the experimental wall temperature profiles have been piecewise constant interpolated and replaced to the constant ones in order to re-calculate a more reliable averaged heat flux profile. Since wall temperature variations are small in both cases, all this process was conducted under the hypotesis of constant convective heat transfer coefficient. In order to compare different results, also an axisymmetric version of this chamber has been analyzed within the same settings, except for cells clustering toward the upper wall. In this case the boundary condition on the upper wall was a ramp of temperature between 410 and 530 K until 220 mm and a constant value of 530 K from there on.

V. Results

A. Wall heat flux

Referring first to the single element combustor case, the experimental values have been obtained from thermocouple readings using an inverse heat conduction problem. No circumferential heat flux distribution is given in the experimental data. Instead an averaged heat flux was used in the reconstruction process. Therefore the experimental values are compared to the circumferential average of the simulations. The experimental data shows a steep rise in the injector near region. After a short drop, that is likely related to a recirculation zone near the faceplate, the heat flux rises continuously until it reaches a plateau near the end of the combustion chamber[11]. The two simulations performed with full flow inlet can not provide a reliable estimation of the experimental results due to the lack of modeling, but their prediction at the throat can be compared with solutions by JAXA and ADS [11]. Within the comparison in fig.4a, the three dimensional full flow solution shows the highest peak of heat flux, which undergoes a wide oscillation along the flat throat due to mixture compressibility phenomena. As expected, in the wall contour plot (fig.4b) the corner zone is characterized by a heat flux tending to zero due to the ambiguity in the determination of the normal versor involved in the temperature gradient. Going to the axisymmetric case, the throat area is preserved, but the shape is clearly different. As a consequence a smaller heat flux occurs. The difference, of about 8 %, is justified by the different throat heights between the two nozzles, resulting in different temperature gradients at the wall. This numerical solution by AFFS is directly comparable with the ADS's one [11]. Although ADS considered detailed injection of propellants and combustion, the peak is almost the same, with a negligible difference. The reason has to be sought in the approach used for chemistry kinetics, in fact ADS uses a combustion model that assumes local chemical equilibrium in every computational cell explaining the high values for the heat output. A finite rate mechanism was used by JAXA, which obtained relatively small values, much more comparable with a completely modeled numerical solution calculated with the present software at DIMA [16]. The latter includes injection and combustion processes. Both solutions work good in approaching the experimental data but differ a little bit at the throat, probably due to the different turbulent Schimidt numbers (0.7 of DIMA and 0.9 of JAXA) and turbulence models.

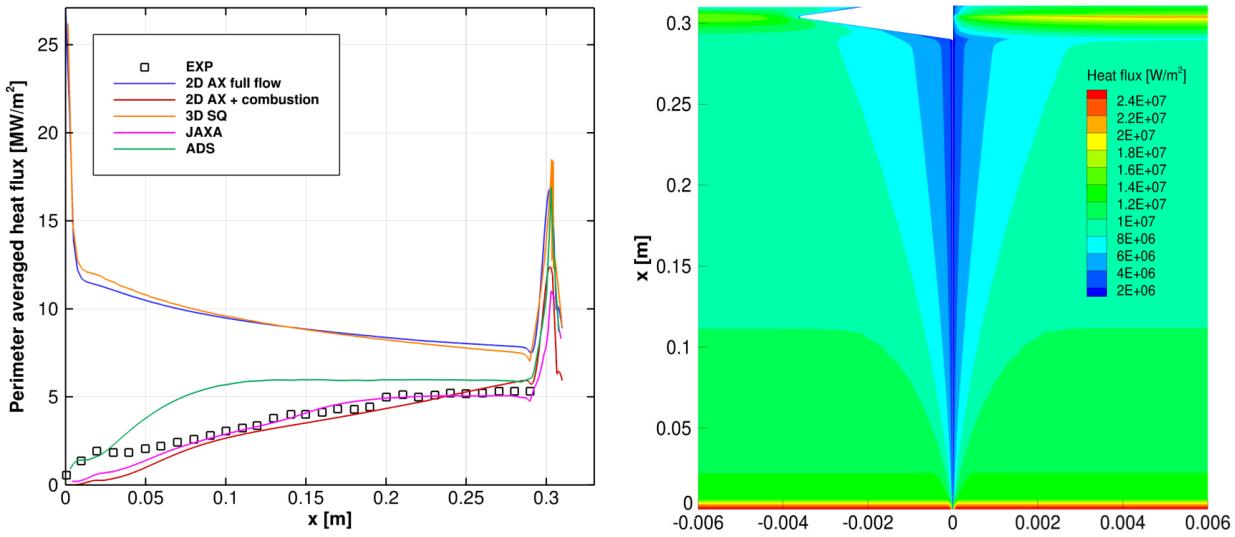

(a) (b)

Fig. 4 (a) Comparison among perimeter averaged heat fluxes; (b) Wall heat flux contour plot for the square/rectangular shaped chamber.

The effect of the combustion and injection processes on heat flux is well explainable by means of temperature fields. The two different solution produced by DIMA result in the temperature fields shown in fig.5. The deviation among peaks of heat flux, quantifiable around 26.3 %, is motivated by a different development of boundary layers within the two fields. A detailed injection promotes a globally thicker boundary layer, in which even relatively low temperatures are visible at the throat although there is an hotter region toward the axis. In case of non detailed injection, the boundary layer is developing as well, but at the throat the average temperature is greater than the previous one.

A similar comparison among heat flux profiles has been done also for the 7 element combustor i.e. the real topic of this work. Since the entire assembly was actively cooled during the experiment, this time averaged throat data are available for comparison thanks to the calorimetric method employed by TUM. In this case, all the solutions taken for comparisons [10] feature injection and combustion. In fig.6 are shown the chamber segments with all the integrated calorimetric wall heat fluxes the full flow solution is compared with. Because of the injection procedure, the values decrease going downstream until the nozzle, whereas literature's results follow the usual trend. Besides the first two values, that are absolutely inconsistent with whichever real application, the values integrated in the third segment show the best agreement within the whole domain because of the intersection between the increasing trend of literature and the decreasing one of this work. Experimental data show clearly that combustion ends completely already between the third and fourth segment, whereas some differences occur among numerical solutions. Roughly speaking, the decreasing trend of the full flow solution match the JAXA one except for a constant amount.

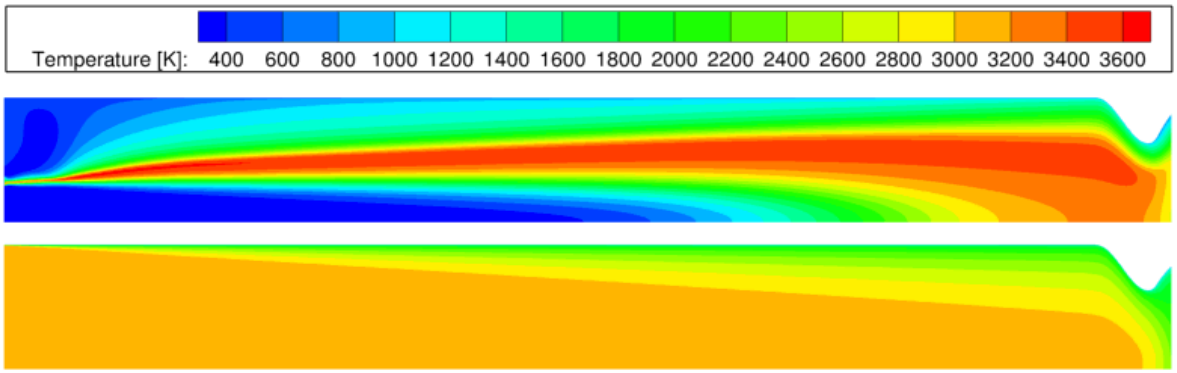

Fig. 5 Temperature fields within single element combustor in case of detailed and non detailed injection by AFFS.

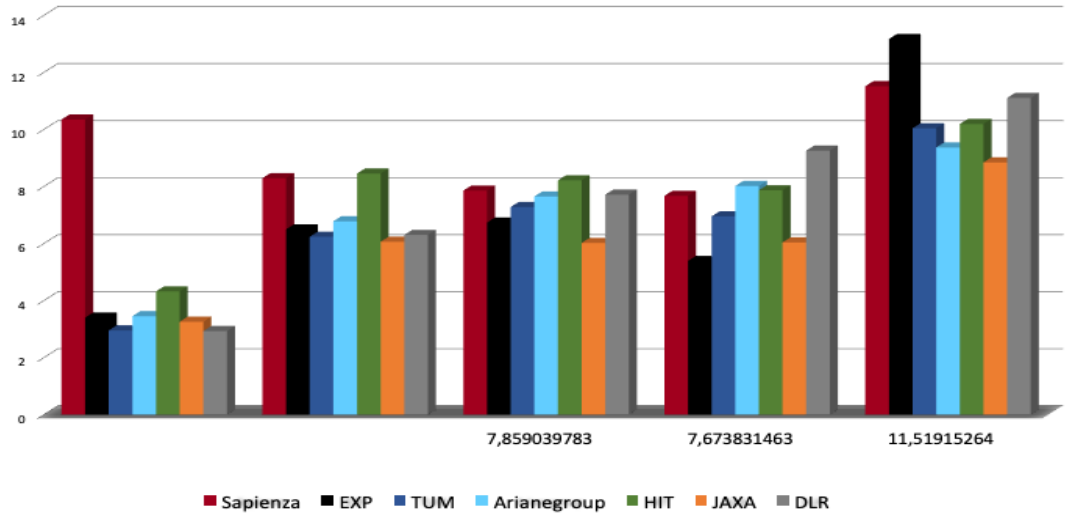

Fig. 6 Integrated heat flux at the 7 element chamber wall (units MW/m^2) [10].

There is not really a good agreement among integrated values at the fourth segment and at throat. All the solutions respectively overestimate and underestimate the experimental value up to a maximum of about 40%. The full flow estimation is the closest one to the reference value, returning in particular an error of 12.4 % as can be seen from the values in fig.6. The explanation for this discrepancy among solutions is attributed to some heat axially transferred from the first to the second cycle of cooling water. In 2018, Daimon et al. studied this same combustor via coupled numerical simulations [9], pointing out that, since the coolant temperature of the inlet for the second cycle is lower than that

of the outlet for the first cycle, the coolant flow of the second cycle receives heat from not only the hot-gas side wall but also the cylindrical part. As a consequence, being a source of energy for the last segment, the fourth one shows a lower integrated heat flux with respect to numerics. In this framework, from Daimon et al.'s study one can estimate that the axial heat transfer partecipates to the hot gas side one by adding a considerable amount, evaluated around 3 MW/m^2. Taking into account probable variations due to the numerical method, thanks to this consideration the full flow estimation of the integrated heat flux in the nozzle can reasonably approach a deviation between 6 and 10 %.

B. Effects of chemical recombinations on heat flux

In order to understand how much recombinations participate to the effective heat load and their role within the boundary layer, a frozen simulation has been performed with the 7 element combustor.

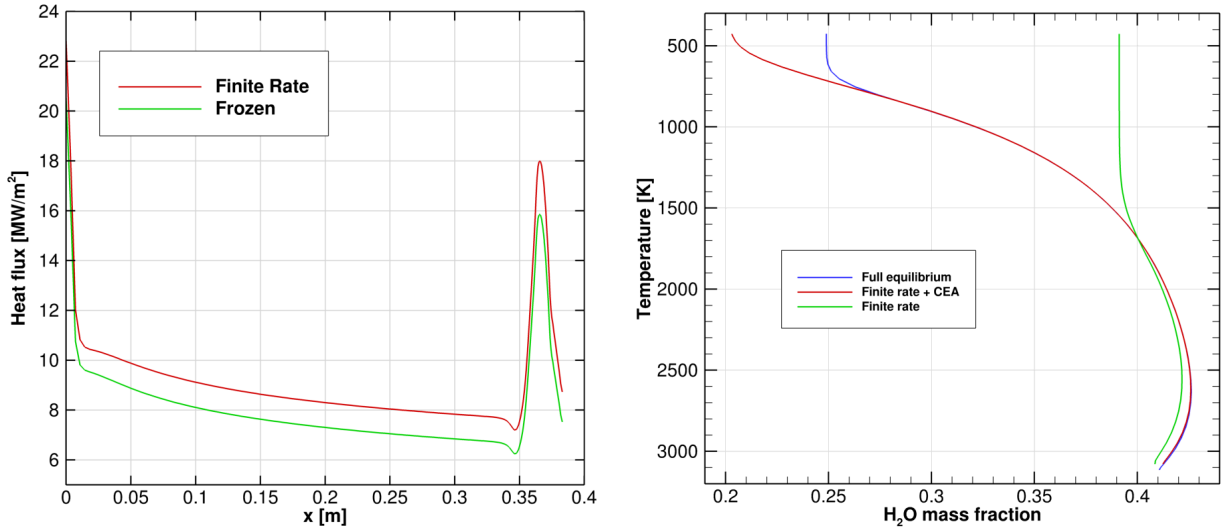

(a) **(b)**

Fig. 7 (a) Comparison among finite rate and frozen convective heat fluxes; (b) H_2O mass fraction radial profile at the throat for different reacting models.

A deviation of about 12 % has been observed at the throat (fig.7a) due to the lower energy release with respect to the reacting model in which a detailed kinetic mechanism applies. Going further, also chemical equilibrium results have been compared to the finite rate ones in order to have informations about the error made by assuming that the flow is always in chemical equilibrium itself. Water mass fraction radial profiles at throat cross section are taken as a reference. The composition changes that affect wall heat flux occur just close to the wall and it has been observed by Betti et al. [13] that this evolution is clearer if analyzed as a function of temperature instead of the radial direction. According to this approach, profiles are plotted in fig.7b. Besides the finite rate solution, chemical equilibrium was achieved in two different ways i.e. by enforcing it in every computational cell of the finite rate solution by means of CEA and increasing the reaction rates by several order of magnitude. Depending on the reacting model, the mixture shows a different freezing point, which moves from 1500 to 500 K. Since recombinations occur completely at chemical equilibrium, the latter is clearly inconsistent and is justified by the numerical limit imposed by chemistry stiffness in increasing the reaction rates. Freezing temperature causes the main error among solutions and affects a lot the production of species within the boundary layer. This error is very considerable as can be seen for water, whose production presents a maximum due to the recombination of its radicals and then a deplection for the formation of CO_2 together with CO. The last two species present similar profiles, characterized by freezing points and steep gradients at chemical equilibrium.

C. Wall temperature

An important aspect to evaluate is if the wall temperature enforced as boundary condition is acceptable or not. As the 7 element combustor test case suggest [5], among selected literature the temperature distribution along the upper wall in non-coupled simulations is determined by an interpolation of thermocouple readings. In this work, for the sake

of simplicity, the wall temperature has been set to a constant value i.e. the furthest reading from the faceplate. The following analysis is based on the fact that thermocouples are collocated within the chamber wall at different positions. Therefore the read value and the actual one at the wall are different. Starting from the piecewise linear interpolated one, the actual wall temperature profile is calculated by means of the numerical heat flux within the thickness in between thermocouples and the wall itself again under the hypothesis of constant convective heat transfer coefficient, as shown in fig.8 and eq.1. The first 8 thermocouples and the remaining 3 are positioned respectively 0.7 *mm* and 1 *mm* away from the hot gas side [5].

$$T_w = \frac{k/\delta \, T_{wr} + h_g T_{aw}}{h_g + k/\delta} \tag{1}$$

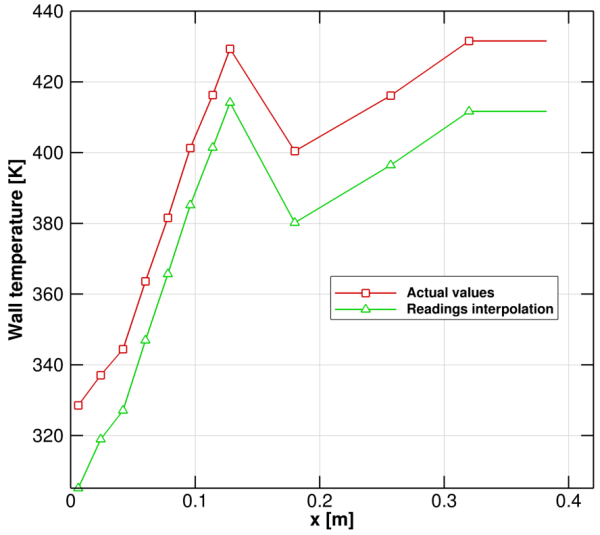

Fig. 8 Wall temperature: piecewise linear interpolation of experimental readings and actual wall values [5].

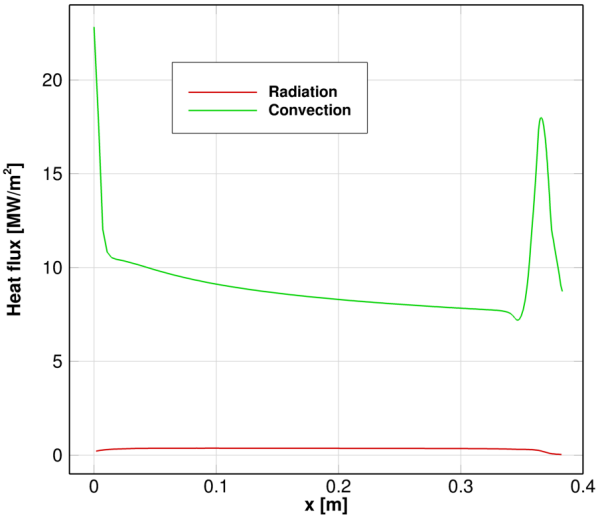

Fig. 9 Comparison beetween convective and radiative heat fluxes.

A great part of the left half of the combustion chamber is characterized by small deviations beetween 15 and 18 *K* except for the first value that, in agreement with the heat flux, is inconsistent with the rest. Going downstream the difference settles at 20 *K* until the end. As a consequence, numerically speaking the imposition of a constant temperature does not cause any problem in the nozzle. This work was thought in order to compare throat heat transfer with other studies, so it is quite indifferent to deviation even of an hundred of kelvins in other chamber regions.

D. Radiation

Besides theoretical concepts, the radiative heat flux has been calculated by a software suitably developed and validated at DIMA [14]. According to fig.9, the heat flux produced by radiation is almost zero in comparison with convection, with a maximum of 0.368 MW/m^2. Such a low value was expected due to the small amount of radiant gas particles in a subscale thrust chamber. Also the low chamber pressure promotes the development of weak radiation, which instead is dominant in big engines.

E. Experimental mass flow rate matching and chamber length variation analysis

Since propellants are injected at chemical equilibrium, a unitary combustion efficiency can be attached to the 7 element combustor full flow simulation. Therefore no total pressure losses occur due to combustion, as instead happens in the experimental tests. Being the chamber pressure enforced as boundary and initial condition in all the simulations so far, as a consequence the mass flow rate should be different. Quantities and derived heat fluxes are shown in fig.10a.

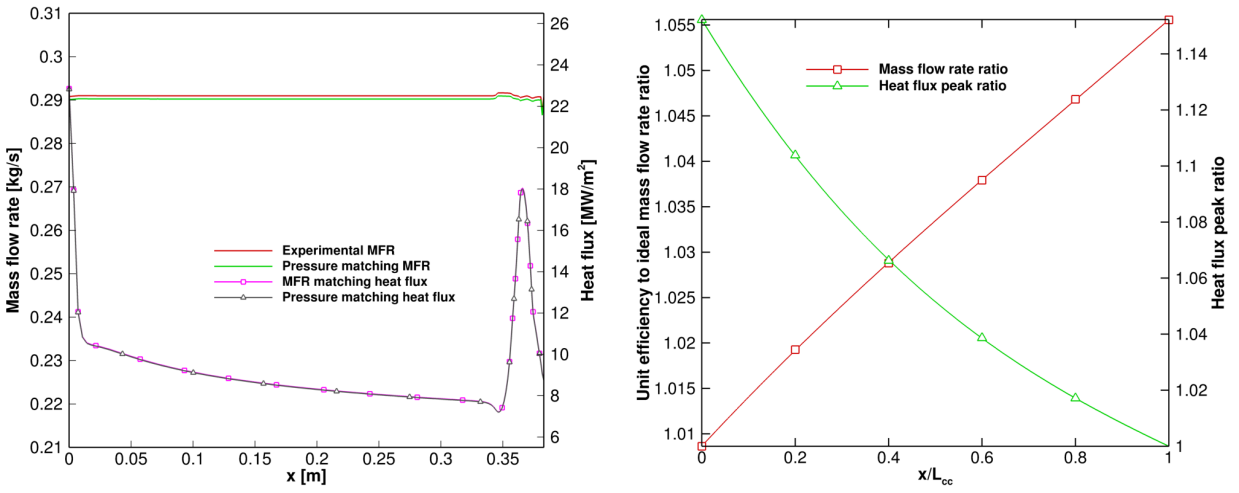

(a) **(b)**

Fig. 10 (a) Mass flow rates and derived heat fluxes under pressure and mass flow rate matching conditions; (b) Mass flow rate and heat flux peak ratios as a function of the combustion chamber length.

Despite total pressure losses, in enforcing the experimental chamber pressure the resulting mass flow rate is almost equal to the experimental one. This strange aspect has been further investigated by checking the average characteristic velocity at specific cross sections. Apparently the experimental test and the full flow solution undergo the same amount of performance losses, but in the first case they occur due to heat release during combustion, whereas numerically the low temperature enforced at the wall causes a decrease by the same amount of characteristic velocity. On the other hand, the same happens trying to recover the experimental mass flow rate by enforcing a suitable chamber pressure. In both cases the mass flow rates are subject to numerical errors toward the nozzle. The derived heat fluxes are almost the same, with a negligible deviation. In general, for a fixed chamber pressure experimental conditions can be matched also according to a graphic approach, in which the mass flow rate is expressed as a function of the combustion chamber length, nozzle excluded. In order to accomplish that, 5 more simulations with varying combustion chamber length have been performed on the same bases for the 7 element combustor, resulting in a very linear-looking cubic dependency, shown in red in fig.10b. Mass flow rates have been normalized with their ideal value of about 0.273 kg/s calculated by CEA. According to the polynomial interpolation, in the graph outer upper part there exists a particular length which returns the experimental mass flow rate. As expected, this length is greater than the original one of 341 mm due to the lower characteristic velocity due, in turn, to the higher mass flow rate. From the same figure one can notice how the mass flow rate tends to its ideal value with reducing combustion chamber length. Actually, a shorter combustion chamber results in a less wide chamber cooling, therefore leading to an increase of performances in terms of characteristic velocity. The same thing has been done with the peak of heat flux, resulting again in a cubic dependency, but with a steeper derivative for short chambers.

F. Error analysis

The three grid levels considered for the 7 element combustor computational grid have been picked up in order to verify grid independence and evaluate the numerical error. The latter has been evaluated by comparing each grid solution to the Richardson extrapolated solution [13], computed as

$$f_{\text{rex}} = f_{\text{fine}} + \frac{f_{\text{fine}} - f_{\text{medium}}}{r^2 - 1} \tag{2}$$

This procedure has been applied both to heat flux and mass flow rate (fig.11) and has succesfully recovered the solver spatial order of accuracy of 2.

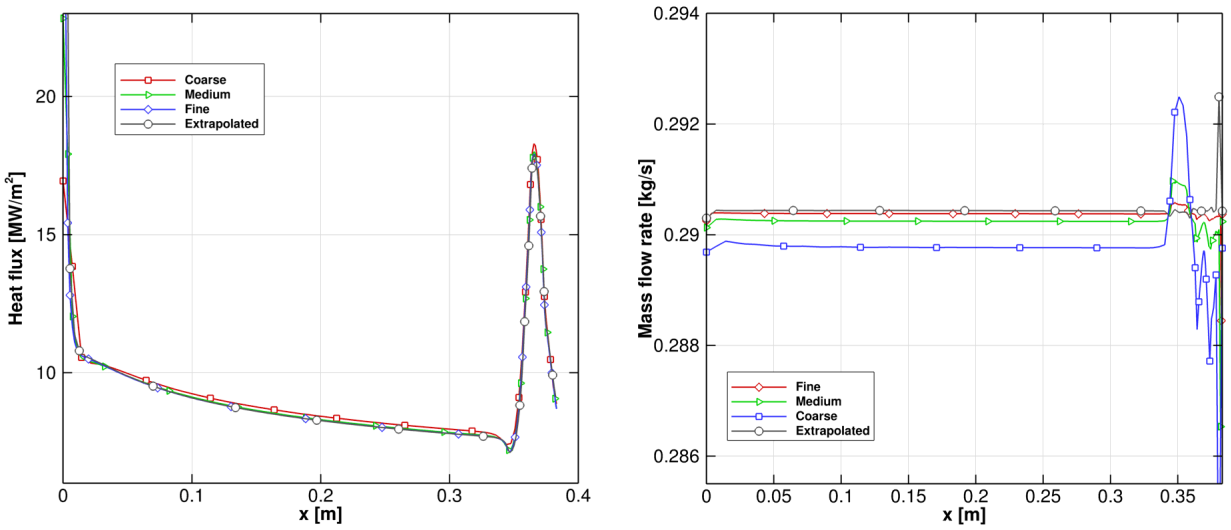

(a) **(b)**

Fig. 11 Asymptotic convergence analysis (rescaled y axes), (a) Heat flux; (b) Mass flow rate.

VI. Conclusions

A non detailed injection process has been employed in order to carry out reliable heat flux CFD predition. The numerical solution and the experimental one differs a lot within the single element combustion chamber due to the lack of modeling, but the first one has been capable to provide reasonably different results at the throat within different settings. A good deviation of 12 % has been found in the 7 element combustor case, whose internal axial heat transfer mechanism turned out as responsible of a considerable increase in the heat load at the hot gas side. Frozen chemistry showed how much recombinations affect the heat load, resulting in a non negligible fraction, again, of 12 %. Freeze temperatures let chemical equilibrium be a rather strong condition in obtain realistic predictions since an exaggerated amount of products are generated together with the resulting heat release. Moerover, the occurring of chemical reactions until wall temperature is inappropriate because a generic temperature layering would never be capable to provide such activation energy. Hence, a detailed kinetic mechanism is strictly required in order to have reliability. On the contrary, radiation as well as the deviation from the actual wall temperature, are totally negligible in this case. Although the absence of total pressure losses due to the unitary combustion efficiency, the reproduction of the experimental conditions seems not to affect the heat flux profiles at all. Leaving this to a coincidence, a parametric analysis with varying chamber length has been conducted in order to understand the role of combustion efficiency within the difference between injection models. Numerical simulations have been demonstrated how neglecting injection and combustion processes can be globally an acceptable simplification also in case of subscale chambers. Although the vicinity of the faceplate can not be correctly analyzed, the full flow approach has been capable to predict the heat flux at the throat with reasonable deviations with respect to more complete models adopted in literature, DIMA included. Significant lack of modeling can be identified relying on the chamber length variation. Longer chambers allow the heat flux immediately upstream to the nozzle to be smaller, even the same of that in case of a detailed injection according to a suitable length. The wider wall and, consequently, the stronger chamber cooling are responsible for a thicker thermal stratification which limits significantly the hotter flow region extent and so the heat transfer. Although similar nozzle inlet conditions can be achieved, the more developed boundary layer limits also the throat heat load, certainly leading to a significant deviation with respect to the full modeled case. Further examinations of the 7 element combustor experimental test are planned in the immediate future also by DIMA. It may be interesting to study even a coupled simulation, in which the actual contribution of the axial load can be quantified, adjusting a little bit the estimation given in this work. Some kind of different patterns of injectors may be used to have comparisons with other literature or, hopefully, in order to expand the competencies about the oxygen/methane propellant combination.

VII. Acknowledgements

The author would like to thank his thesis advisor Prof. Francesco Nasuti for all the support and the huge amount of acquired competencies.

References

[1] Cook, R. T., "Methane heat transfer investigation," 1984.

[2] Celano, M., Silvestri, S., Schlieben, G., Kirchberger, C., Haidn, O., and Knab, O., "Injector characterization for a gaseous oxygen-methane single element combustion chamber," *Progress in Propulsion Physics*, Vol. 8, 2016, pp. 145–164.

[3] Perakis, N., and Haidn, O., "Inverse heat transfer method applied to capacitively cooled rocket thrust chambers," *International Journal of Heat and Mass Transfer*, Vol. 131, 2018, pp. 150–166. doi:10.1016/j.ijheatmasstransfer.2018.11.048.

[4] Haidn, O., Knab, O., Celano, M. P., Silvestri, S., Kirchberger, C., and Schieben, G., "Transregio SFB/TR R40 Test Case 1," *Technical Report*, 2015.

[5] Haidn, O., Silvestri, S., Celano, M. P., and Roth, C., "Transregio SFB/TR R40 Test Case BKS-2," *Technical Report*, 2016.

[6] Burkhardt, H., Sippel, M., Herbertz, A., and Klevanski, J., "Kerosene vs. methane: a propellant tradeoff for reusable liquid booster stages," *Journal of Spacecraft and Rockets*, Vol. 41, No. 5, 2004, pp. 762–769.

[7] Sharma, A., and Kumar, S. S., "LOX-METHANE COMBUSTION CHARACTERISTICS IN SWIRL COAXIAL INJECTOR OF LOX-HYDROGEN ENGINE," 2018.

[8] Neill, T., Judd, D., Veith, E., and Rousar, D., "Practical uses of liquid methane in rocket engine applications," *Acta Astronautica*, Vol. 65, No. 5-6, 2009, pp. 696–705.

[9] Daimon, Y., Negishi, H., Silvestri, S., and Haidn, O. J., "Conjugated Combustion and Heat Transfer Simulation for a 7 element GOX/GCH4 Rocket Combustor," *2018 Joint Propulsion Conference*, 2018, p. 4553.

[10] Perakis, N., Haidn, O. J., Eiringhaus, D., Rahn, D., Zhang, S., Daimon, Y., Karl, S., and Horchler, T., "Qualitative and Quantitative Comparison of RANS Simulation Results for a 7-Element GOX/GCH4 Rocket Combustor," *2018 Joint Propulsion Conference*, 2018, p. 4556.

[11] Roth, C., Haidn, O., Chemnitz, A., Sattelmayer, T., Frank, G., Müller, H., Zips, J., Keller, R., M. Gerlinger, P., Maestro, D., Benedicte, C., Riedmann, H., and Selle, L., "Numerical Investigation of Flow and Combustion in a Single Element GCH4/GOx Rocket Combustor," 2016. doi:10.2514/6.2016-4995.

[12] Perakis, N., Rahn, D., Eiringhaus, D., and Haidn, O., "Heat Transfer and Combustion Simulation of a 7-Element GOX/GCH4 Rocket Combustor," 2018. doi:10.2514/6.2018-4554.

[13] Betti, B., Bianchi, D., Nasuti, F., and Martelli, E., "Chemical reaction effects on heat loads of CH4/O2 and H2/O2 rockets," *AIAA Journal*, Vol. 54, No. 1, 2016, pp. 1693–1703.

[14] Leccese, G., Bianchi, D., Betti, B., Lentini, D., and Nasuti, F., "Convective and radiative wall heat transfer in liquid rocket thrust chambers," *Journal of Propulsion and Power*, Vol. 34, No. 2, 2017, pp. 318–326.

[15] Leccese, G., "Gas-Surface interaction, radiative heat transfer and thermochemistry modeling in the simulation of paraffin-based hybrid rocket engines," Ph.D. thesis, Ph. d. dissertation, Univ. of Rome'La Sapienza'Rome, 2017.

[16] Nasuti, F., Frezzotti, M. L., and Concio, P., "Numerical estimations of peak heat flux at throat of liquid rocket engines," *32nd International Symposium on Space Technology and Science (ISTS), & 9th Nano-Satellite Symposium (NSAT), Fukoi, Japan*, 2019.